Title

The Ultrafast Dynamics of Image Potential State Electrons at the Dimethylsulfoxide/Ag(111) Interface

Authors

Strader, Matthew L.
Garrett-Roe, Sean
Szymanski, Paul
et al.

Publication Date

2008-04-08

The Ultrafast Dynamics of Image Potential State Electrons at the Dimethylsulfoxide/Ag(111) Interface

Matthew L. Strader, Sean Garrett-Roe,[α] Paul Szymanski,[β] Steven T. Shipman,[γ] James E. Johns, Aram Yang, Eric Muller, Charles B. Harris[*]

Department of Chemistry, University of California, Berkeley, California 94720 and Chemical Sciences Division, Lawrence Berkeley National Laboratory, Berkeley, California, 94720

α Current address: University of Zurich, Physikalisch-Chemisches Institut, Winterhurerstrasse 190, 8057 Zurich, Switzerland.
β Current address: Chemistry Department, Brookhaven National Laboratory, Upton, NY 11973.
γ Current address: Department of Chemistry, University of Virginia, Charlottesville, VA 22904.
* Corresponding author: Tel: (510)-642-2814; Fax: (510)-642-6724; cbharris@berkeley.edu

Abstract

Angle-resolved two-photon photoemission was used to study the energy relaxation, population decay and localization dynamics of image potential state (IPS) electrons in ultrathin films of dimethylsulfoxide (DMSO) on an Ag(111) substrate. Dynamic energy shifts of 50 ± 10 meV and 220 ± 10 meV were observed for n=1 IPS electrons at one monolayer and two monolayer coverages of DMSO, respectively. The difference in energy shifts is attributed to rotational hindrance of the molecular dipole in the chemisorptive first monolayer. The finding confirms the proposed mechanism for the low differential capacitance of dimethylsulfoxide at noble metal interfaces in solution. A novel description of the IPS as a surface capacitance is presented to facilitate comparisons with electrochemical systems.

Keywords: photoemission, surface science, capacitance, solvation, ultrahigh vacuum

Introduction

In electrochemically relevant systems, interfacial capacitance affects signal collection and heterogeneous charge transfer.[1-3] Charge accumulation at the contact surface occurs when materials of dissimilar chemical potentials and/or applied voltage biases are unable to attain electronic equilibrium through interfacial charge transfer (i.e. conduction or faradaic current). Charge is stored by an electrolyte concentration gradient and dielectric solvent reorganization on the solution side of the interface and by electron accumulation at the electrode surface. This system is commonly referred to as the electrochemical double layer. The charge storage properties of the double layer can be described as capacitor-like in nature, with the notable deviation from a classical capacitor being the potential-dependent capacitance. A standard definition describing double layer capacitance is the differential capacitance (C_d) and is given in Equation 1 in terms of the surface charge (Q) and applied potential (V).[4]

$$C_d(V) = \frac{\partial Q}{\partial V} \qquad (1)$$

Several models of the electrochemical double layer, including the Helmoltz, Gouy-Chapman, Gouy-Chapman-Stern and jellium descriptions have been used to varying degrees of success in the study of interfacial capacitance, spanning over a century of research.[5-9]

Dimethylsulfoxide (DMSO), a common electrochemical solvent, exhibits an uncharacteristically low differential capacitance at noble metal electrodes (7-10 $\mu F/cm^2$ over a 1.5 V range including the potential of zero charge). Similar, polar, high-dielectric constant electrochemical solvents can show differential capacitances much higher (50 $\mu F/cm^2$ for acetonitrile under identical experimental conditions).[10] DMSO interacts chemisorptively with noble metal surfaces.[10] Both the oxygen and sulfur sites interact

strongly with the metal to cause displacement of electrolytes and other solvents from the surface in solution. Hindered rotation of the DMSO dipole has been proposed to reduce the interfacial DMSO response to potential changes and lower its interfacial capacitance,[10, 11] in accordance with established double layer theory.[12] As we will demonstrate, this mechanism can be directly tested by comparing the dielectric response of the chemisorptive monolayer with that of various multilayer coverages using two-photon photoemission in an ultra-high vacuum environment.

Ultra-high vacuum (UHV) thin-film interfaces have been used to simulate the electrochemical double layer for decades.[13] This formulation allows interfacial characterization methods to be employed that are incompatible with immersed electrode systems. Several UHV techniques can provide valuable energetic and structural information to complement immersed electrode results. However, vastly different conditions in the immersed electrode and UHV environments, including disparate temperature ranges and variations in surface morphology, can make extraction of relevant data difficult.[14] Despite these limitations, numerous studies have shown relevance of electrochemical information accessible from UHV interfaces.[15, 16]

UHV studies of electron population dynamics, energy relaxation, band structure and localization phenomena are commonplace for a large variety of metal-dielectric interfaces using two-photon photoemission (2PPE).[17-21] 2PPE can access interfacial electronic states and track the dielectric response of adsorbed thin films. A sub-hundred femtosecond pulse and its second harmonic impinge upon an Ag substrate with a controllable time delay of femtoseconds to picoseconds between pulses. The initial pump pulse excites an electron from below the Fermi level to an intermediate state from which the electron is later photoemitted. Knowledge of the probe photon energy, the electron

kinetic energy after photoemission and the time delay between pump and probe pulses provides the data to study the time dependence of the binding energy.[22, 23]

In 2PPE, the states populated by a UV pump are the hydrogenic progression of IPS's arising from the attractive, coulombic potential between an electron and the polarization it induces at a metal surface. The IPS binding energy is given by Equation 2:

$$E_n = -\frac{.85\text{eV}}{(n+a)^2} + V_0 \qquad (2)$$

where n represents the principle quantum number, V_0 represents the vacuum energy and a represents the quantum defect parameter.[22] The dynamic binding energy shift can result from changes in the dielectric response of the adsorbed layer to the image potential electron. This manifests itself as a dynamic, local workfunction shift induced by changes in the adsorbed layer.[22, 24] Consequently, the IPS proves a useful probe of the layer's time-dependent dielectric response.

Additionally, the electron dispersion in a direction parallel to the surface can be measured. Electron momentum parallel to the surface of the metal ($\mathbf{k}_\parallel$) is conserved upon photoemission, and $\mathbf{k}_\parallel$ can be obtained from momentum conservation using Equation 3:

$$k_\parallel = \frac{\sqrt{2m_e E_{kin}}}{\eta}\sin\theta \qquad (3)$$

where θ is the angle at which electrons are photoemitted with respect to the surface normal, E_{kin} is the measured kinetic energy of the electron, and m_e is the mass of a free electron.[25] The dispersion of a delocalized electronic state is characterized by its kinetic energy as a function of parallel momentum and is given by Equation 4:

$$E_{kin}(k_\parallel) = E_{kin}(0) + \frac{\eta^2 k_\parallel^2}{2m^*} \qquad (4)$$

where m^* denotes the electron effective mass and is related to the curvature of the band.[26]

Electrons at interfaces have shown dynamic m^* shifts and/or localization over time.[23, 27] The kinetic energy of an electron photoemitted from a localized state is invariant to collection angle and does not display the $\mathbf{k}_\parallel$-dependence of a delocalized state described by Equation 4. The localized state can be described by a weighted sum of plane waves,

$$\psi_{loc} = \sum_{k_\parallel} c_{k_\parallel} \psi_{k_\parallel} \qquad (5)$$

and an electron in this state no longer possesses a unique $\mathbf{k}_\parallel$.[28] The photoemission angle does not accurately reflect the momentum of the state, but the distribution of the coefficients does describe the shape of the localized state in **k**-space. The **k**-space width is related to the wavefunction size distribution in coordinate space, and a rough estimate of its size can be made. It can be shown that the Gaussian full width at half maximum (FWHM) in coordinate and momentum space are related by a Fourier transform given by Equation 6.[28]

$$\Delta x_{FWHM} = \frac{4 \ln 2}{\Delta k_{FWHM}} \qquad (6)$$

Experimental

Sigma-Aldrich anhydrous grade DMSO (≥99.9% DMSO, ≤0.005% water) was transferred to a glass bulb in a nitrogen environment and attached to a high vacuum line (~5×10^{-7} torr). Multiple freeze-pump-thaw cycles were performed to remove residual impurities, and DMSO purity was verified by a quadrupole mass spectrometer in the main UHV chamber. The main UHV chamber containing the Ag(111) crystal was

backfilled with DMSO from the vacuum line via a variable leak valve. Main chamber pressure and exposure times were recorded, and dosing is reported in units of Langmuir (1 Langmuir ≡ 1 μtorr x 1 s). All reported ultrathin films were dosed at an uncorrected pressure of 3.5×10^{-8} torr. Substrate temperatures of 210 K and 200 K were used for monolayer and thicker coverage growth, respectively.

The Ag(111) single crystal was prepared prior to DMSO exposure with Ar^+ ion sputtering (500 K, 500 eV, 5×10^{-5} torr) followed by annealing at 725 K in an UHV environment. Surface quality and purity could be verified by LEED and Auger spectroscopy as well as 2PPE dynamics scans.

The laser system used to collect 2PPE data has been described in detail elsewhere.[29] The relevant features are a laser that generates <100 fs FWHM pulses at 200 – 250 kHz of tunable wavelengths from 490 – 740 nm. These pulses are frequency doubled, producing ~10 nJ and ~20 nJ pulses for the frequency double and residual fundamental wavelengths, respectively. The fundamental (vis) pulse is split from the second harmonic (UV) pulse by a dichroic mirror and delayed by a translation stage with one micron (6.7 fs) step size.

All photoemission data were collected with a time-of-flight electron detection system described previously.[26] A controllable voltage bias was applied to compensate for contact potential shifts due to adsorption. A background spectrum was acquired at 3.3 ps and subtracted from all time-dependent spectra to remove single pulse photoemission mechanisms (i.e. UV-UV, vis-vis-vis). 2PPE spectra were collected with wavelengths 720 nm or longer to avoid significant one-photon photoemission.

Results

Angle-resolved dynamics were collected for monolayer and multilayer coverages of DMSO adsorbed on Ag(111) at angles from 0° to 24° in 4° increments. The results for 0° and 24° dynamics are presented in Figure 1 for 1 ML and 2 ML coverages. Two peaks corresponding to the n=1 and n=2 IPS were identified in 1 ML spectra. Three peaks were identified in the 2 ML spectra, which corresponded to initially populated, delocalized n=1 and n=2 IPS's and a dynamically-formed localized state. In both the 1 ML and 2 ML spectra, the n=2 peak dispersed to energies near the pump photon energy at high collection angles and was therefore truncated.

Kinetic energy spectra were corrected for inelastic scattering using the Shirley function,[30] a background subtraction method originally applied to x-ray photoemission spectra and later extended to UV and visible photoemission data.[29, 31] The Shirley function effectively removes the low-energy inelastic tail, evident in Figure 2 spectra, and the resulting lineshape asymmetry using only one free parameter: a proportionality constant. All figures present spectra corrected for inelastic scattering unless otherwise noted. Peaks identified by dosing survey and dispersion data were fit to Voigt functions The area under a Voigt is proportional to the total population of electrons photoemitted from the electronic state. The population of electrons collected at a given photoemission angle could consequently be plotted as a function of time to study population decay dynamics. Similarly, the time-dependent energetic position of a peak yielded energy relaxation dynamics. All measurements include error bars as an assessment of instrument error, not as a rigorously defined standard deviation, unless stated otherwise.

Coverage identification

Dosing surveys were performed to identify monolayer and multilayer coverages, in conjunction with subsequent measurements. Experimentally, exposures were limited to a minimum of 0.35 L due to the previously observed low pumping rate of DMSO from the UHV chamber.[10] The results of a survey using minimum exposure increments are presented in Figure 2 with all spectra referenced to the monolayer vacuum energy and with no correction for inelastic scattering. The energy gap between the Fermi level and the clean Ag n=1 IPS was larger than the pump pulse energy; consequently, the only clean Ag features observed were the *sp* bulk transition and the low energy tail of the Shockley surface state.[30]

As DMSO was dosed at 210 K, a new feature, the n=1 IPS, was observed to grow in and saturate, which is displayed in the spectrum labeled 0.7 L of exposure in Figure 2. Subsequent dosing at this temperature produced no further changes in 2PPE spectra or dynamics. Time-resolved scans of this coverage, however, indicated small traces of the long-lived, localized multilayer state. The coverage assigned as monolayer could only be reached after annealing the saturated coverage for 10 min at 210 K, presumably to remove small multilayer patches adsorbed at favorable nucleation sites. After annealing, no features were present from either the multilayer or the clean Ag surface. The necessity of annealing to obtain a monolayer is qualitatively in agreement with the literature.[10, 32] Subsequent dosing at 200 K produced multilayer coverages. Multilayer thickness is reported in monolayer equivalences (ML) using a monolayer exposure of 0.5 ± 0.1 L. This value for monolayer exposure was obtained by observing saturation at

210 K in subsequent experiments with larger exposure increments. Thickness above 1 ML should be treated as a measure of average exposure, not as an assumption of layer-by-layer growth. Equation 2 was used to calculate a –1.20 ± 0.03 eV workfunction shift from 1 ML of DMSO and an additional +0.12 ± 0.03 eV from 2 ML of DMSO with quantum defect parameters of 0.1 and 0.15, respectively.

Monolayer Dynamics

A monolayer coverage of DMSO was characterized by a dispersive, short-lived, n=1 IPS which showed little solvation. The n=1 IPS peak was fit to one Voigt function at all angles, and its effective mass was determined to be 1.5 ± 0.1 m_e and 1.7 ± 0.3 m_e at pump-probe delays of 0 fs and 167 fs, respectively. The curvature is most evident at higher photoemission angles, where the energy shift is significantly larger than the experimental energy resolution.[29, 33] No evidence of dynamic localization was observed, as shown in Figure 3. Population dynamics were adequately fit to a monoexponential rise and decay[34] at all collection angles and convoluted with a Gaussian representing the instrumental response function. The data and corresponding fits for the 1 ML coverage at 0° and 24° are presented in Figure 4. Population decay times were found to be short at all collection angles, and the longest decay time of τ = 48 ± 15 fs was observed at 0°. Population rise times were found to be much shorter than our experimental response at all collection angles. The 1 ML solvation response was found to be small with a total energy shift of 50 ± 10 meV observed at 0°. A standard model of solvation by bulk solvents fits the response to a Gaussian and one or more exponentials.[35] The data bore little resemblance to a Gaussian, an exponential or combination thereof, as evidenced in

Figure 5. A straight line was empirically selected to fit the solvation response at all angles, and the solvation line slopes for various collection angles of the 1 ML coverage are summarized in Table 1 with error bars of ± 0.03 eV. Extrapolation of the solvation fit to 420 fs, the time for 95% energy relaxation of a 2 ML coverage, yields a total energy shift of 110 ± 20 meV at 0'.

Multilayer Dynamics

A 2 ML coverage of DMSO was characterized by a long-lived, dynamically localizing, n=1 IPS which exhibited a large solvation response. The dynamic localization is shown in Figure 6, which shows an initially delocalized IPS with an effective mass of 1.2 m_e fully collapsing into a localized state with a slightly negative dispersion by 800 fs. The delocalized n=1 IPS and the localized state were well-resolved at 20° and 24° collection angles and could be cleanly fit to two peaks. Extraction of population and solvation information from the spectrally overlapped delocalized and localized states at the intermediate 12° and 16° collection angles was accomplished with the treatment of the data outlined in the Supporting Information. The separation of localized and delocalized features was not possible at collection angles lower than 12°.

A monoexponential rise and decay function convoluted with a Gaussian was fit to the delocalized and localized state population dynamics. The two time constants were equal within experimental error at every collection angle for the delocalized state; consequently an assignment of one constant as a rise time and the other constant as a decay time was not possible.[34] The average of the two constants is reported in Table 2. A rise time of τ = 100 ± 15 fs and a decay time of τ = 460 ± 40 fs was obtained for the

localized state population dynamics measured at 24°, and the data and the fit are displayed in Figure 4.

The 2 ML solvation response was found to be large with a total energy shift of 220 ± 10 meV observed at 0°, displayed in Figure 5. The 2 ML delocalized state exhibited a time-dependent energy relaxation best fit to a straight line at collection angles of 12° and larger. For the data collected at 12°, 16°, 20° and 24°, the localized state energy shift was adequately fit to a single exponential, but the standard model of a Gaussian and an exponential component was also tested and found unnecessary. As discussed in the Supporting Information, the localized state exponential relaxation times and Gaussian widths are expected to be invariant to photoemission angle. The exponential relaxation time averaged across collection angles was 140 fs with a 15 fs standard deviation using a single exponential relaxation.

Discussion

Population decay times

The 2 ML IPS clearly decayed back to the metal on a much longer timescale than the 1 ML IPS. This behavior was consistent with a number of systems in which electrons were pushed to the outside of the adsorbed layer, and the additional tunneling barrier hindered efficient decay to the metal,[36, 37] and a 3 ML coverage was examined to verify this mechanism. A monoexponential rise and decay were inadequate to fit population decay, and a biexponential decay produced a much better fit than a stretched exponential. Decay times of $\tau = 440 \pm 40$ fs and $\tau = 5.6 \pm 0.5$ ps were calculated for the 3 ML

localized state at 24°. An order of magnitude decay time increase is expected when pushing the electron 1 ML further from the metal surface. The 3 ML decay time confirms that the IPS resides outside the adsorbed DMSO coverage. Additionally, the 2 ML delocalized state decay times are significantly greater than the 1 ML decay times, despite the additional decay channel via localization, which further supports the conclusion that IPS electrons are pushed to the outside of the adsorbed layer.

Dynamic energy relaxation mechanisms

An analysis of interfacial electron population and energy relaxation dynamics at D_2O/Ru(001) and D_2O/Cu(111) interfaces has conclusively shown energy relaxation that does not result from solvation,[38] and this mechanism must be considered in the context of the current results. Solvation-independent energy relaxation can occur when decay times of interfacial electrons are faster for higher energy states. A dynamic shift of peak maximum to lower energies is observed as higher energy contributions to an inhomogeneously broadened peak decay more quickly than lower energy contributions. All population decay dynamics of an inhomogeneously broadened peak resulting from this mechanism will lie within the peak envelope of the feature at its maximum population. A dynamic shift of the feature outside of the peak envelope reflects a real energy shift of the inhomogeneous distribution, and another mechanism, i.e. solvation, must be included. Using this criterion, the energy relaxation observed in 1 ML of DMSO could be wholly attributed to energy-dependent decay times. The 2 ML data stands in contrast: both the localized state observed at 24° and the combination of solvated features observed at 0° dynamically shift significantly outside their peak envelopes. In summary,

the 2 ML coverage exhibits solvation, while the 1 ML coverage might not solvate. The following section attributes all energy relaxation to solvation; a complete lack of monolayer solvation would underscore these results.

The image potential state as a capacitance

Molecular dipole reorientation has previously been shown to cause dynamic energy relaxation of IPS's in UHV experiments.[22, 23] A rotationally frustrated monolayer molecular dipole has been previously proposed to explain the low interfacial capacitance of DMSO measured by electrochemistry. The unifying physical process connecting bulk DMSO electrochemical capacitance to the dynamic energy relaxation measured in this experiment is molecular dipole reorientation. Electrochemical measurements obtain bulk values for the entire solvent, and the variation of experimental parameters can be used to draw conclusions about monolayer (Helmholtz layer) and multilayer (Gouy-Chapman layer) contributions. A 2PPE experiment is able to separately study monolayer and multilayer coverages and directly observes layer-dependent dielectric response to injected charge. Across the shared time range when both 1 ML and 2 ML features were observable, the 2 ML response was significantly greater. The 2 ML response was also significantly greater than the 1 ML response extrapolated to 420 fs, the time required for 95% energy relaxation in a 2 ML coverage. The smaller solvation response of the monolayer compared to the 2 ML multilayer is due to the decreased rotational reorientation of the monolayer coverage. The frustrated monolayer reorientation inferred from bulk measurements is evident in this experiment, which draws an explicit connection between in situ measurements and our model electrode interface.

In an attempt to draw an analogy between electrochemical interfacial capacitance and the energy shifts due to solvation, a simple model for the dynamic energy shift is suggested. One should not take this model in any quantitative sense, but rather we develop it more for its pedagogical value. The IPS consists of a charge separation between the electron and its image. This charge separation is held at a potential corresponding to the spacing between the Fermi level and n=1 IPS. Viewed in this context, the IPS and its image could be considered as a capacitance. We will recast the solvation dynamics in the context of capacitance and the dielectric constant.

As an example of the capacitive nature of the system, a simple prediction of the size distribution of IPS electrons at the Ag(111)/vacuum interface is made. Equation 7 states capacitance (C) in terms of charge (Q) and potential (V) and in terms of the vacuum permittivity (ε_o), the dielectric constant (ε), plate area (A) and plate spacing (d) for a parallel-plate capacitor configuration.

$$C = \frac{Q}{V} = \varepsilon_o \varepsilon \frac{A}{d} \qquad (7)$$

A gross assumption of homogeneous electron and image charge distributions across a given surface area (A) at the surface normal direction IPS expectation value (d) reduces the IPS and its image to the parallel-plate situation. Inserting known, measurable quantities for charge, potential, vacuum permittivity, a dielectric constant of one and the expectation value for n=1 in the surface normal direction, Equation 7 predicts a plate diameter of 14 Å.

The dielectric constant used in Equation 7 can be separated into three components of dielectric response for generic media, as specified in Equation 8.

$$\varepsilon = \varepsilon_{ion} + \varepsilon_{mol} + \varepsilon_{el} \qquad (8)$$

The ionic component (ε_{ion}) is non-existent in the current experiment. The electronic component (ε_{el}) occurs on a timescale faster than our 2PPE measurements can detect[39] and does not contribute to the dynamic response. Only the molecular component (ε_{mol}), consisting of dipole rotation and molecular vibrations, contributes to the dynamic dielectric response measured by the current experiment.

Energy relaxation times due to ε_{mol} are highly solvent dependent in bulk solution and can be in excess of nanoseconds. However, DMSO exhibits relatively rapid solvation as observed by Horng *et al.* from the time-resolved Stokes shift of coumarin 153 in DMSO solution,[35] which is consistent with other solvents that lack a hydrogen bond network. They find that the majority of the energy relaxation is described with a 0.214 ps exponential decay time, and the longest decay time of 10.7 ps comprises less than 10% of the total energy relaxation. The localized state is visible at pump-probe delays as large as 2.2 ps in the 2 ML coverage; therefore, the current experiment has access to the time range in which 75% of the ε_{mol} dielectric response occurs in bulk.[35] However, the current experiment is conducted in the presence of an interface at temperatures much reduced compared to the bulk solvent, which could potentially introduce new librational modes and slow large-scale collective solvent motions.

A capacitance can be calculated at a pump-probe delay of 0 fs from the n=1 IPS energy above the Fermi level. This effectively measures the capacitance before the ε_{mol} component can contribute to energy relaxation. A long-time capacitance measurement probes capacitance after complete relaxation from the ε_{mol} contribution. This

circumstance is equivalent to measuring the capacitance between two plates with and without a dielectric medium of ε_{mol} between them. The situation is described by Equations 9:

$$C_i = \varepsilon_{el} C_{vac} \qquad (9a)$$

$$C_f = \varepsilon_{el} C_{vac} + \varepsilon_{mol} C_{vac} \qquad (9b)$$

where the 0 fs capacitance (C_i) and long-time capacitance (C_f) are defined relative to C_{vac}, the capacitance without a dielectric. Simple substitution eliminates the unmeasured C_{vac} term and expresses ε_{mol} as a fraction of ε_{el} in Equation 10.

$$\frac{C_f}{C_i} = 1 + \frac{\varepsilon_{mol}}{\varepsilon_{el}} \qquad (10)$$

In the context of the DMSO results, instantaneous and long-time capacitance measurements can be used to determine the ε_{mol} contribution in terms of ε_{el} for various DMSO coverages. A reasonable value for ε_{el} of 2.19 can be obtained for DMSO by equating ε_{el} to the dielectric response high frequency limit (ε_∞), which is derived using $\varepsilon_\infty \approx n_D^2$ from the index of refraction (n_D).[35] Insertion of the ε_{el} value allows for ε_{mol} determination from the observed, fractional $\varepsilon_{mol}/\varepsilon_{el}$.

Capacitance and ε_{mol} were calculated for the 1 ML and 2 ML coverages and summarized in Table 3. It is curious to note the similarity of long-time capacitances between both coverages, however the combination of effects by which this circumstance occurs implies coincidence. Initial capacitances (C_i), and presumably C_{vac}, are distinct between coverages, which result from the differing static workfunctions of the 1 ML and 2 ML coverages. The higher initial energy of the n=1 IPS in the 2 ML coverage, due to the larger workfunction, is countered by the larger ε_{mol} of the 2 ML coverage. Consequently, the final energy above the Fermi level of the solvated electron in the 2 ML

coverage is equal to the energy of the solvated electron in the 1 ML coverage from the combination of static workfunction and dynamic ε_{mol} contributions.

A variety of treatments were employed to report the data more accurately. The 1 ML coverage showed no long-time asymptote. A range of long-time capacitances for the 1 ML coverage was established by defining two limiting cases. The lower limit was defined by the capacitance at the longest measurable pump-probe delay; long-time IPS energy could not be higher than this value. The upper limit was obtained by considering the solvation timescale of the 2 ML coverage. The molecular response of the monolayer directly adsorbed to the substrate contributes to the observed energy relaxation of the 2 ML coverage. Consequently, the long-time asymptote in the 2 ML energy relaxation dynamics demonstrates the complete relaxation of the directly adsorbed monolayer. While the increased distance and dielectric screening between an electron and the directly adsorbed monolayer in a 2 ML coverage might affect the monolayer relaxation magnitude and could lengthen the relaxation timescale of the adsorbed monolayer with respect to the 1 ML coverage, the asymptotic energy relaxation defines an upper limit for the monolayer solvation timescale. The extrapolation of the monolayer linear solvation response to the 3τ relaxation time of the 2 ML coverage (420 fs) provides a potential from which a capacitance upper limit is calculated. The true long-time capacitance resides within these limits.

Capacitances for the 2 ML coverage were calculated using dynamics collected at 0°. At this collection angle, the delocalized n=1 IPS and the localized state could not be resolved, and one Voigt function fit the combination of these features. Ideally, the delocalized n=1 IPS energy relaxation dynamics collected at 0° would be used. This collection angle was chosen to eliminate potential contributions of dynamic effective

mass shifts to observed energy shifts. If this consideration were ignored, the localized state collected at 24° exhibits an energy shift of 190 ± 10 meV from its initial detection at a 90 fs delay time.

Capacitances per area were reported to highlight the magnitude of the capacitance, otherwise obscured by the small model plate area. Estimates of plate area were made from earlier determinations of the coherence lengths of interfacial delocalized electrons (~100 Å)[22] and the ± 2σ width of a 17 Å FWHM Gaussian-shaped localized state.[28] This correction especially affects the 2 ML ε_{mol} computation due to dynamic shrinkage of the model plate via electron localization. Necessarily, the corrected and uncorrected 2 ML ε_{mol} are interpreted as upper and lower limits of the true value.

The results of ε_{mol} calculations recast the conclusion already reached: the 2 ML coverage has a much larger solvation response to excess charge. Uncorrected for plate area considerations, 2 ML of DMSO has an ε_{mol} of 2.0 - 5.2 times that of 1 ML of DMSO. A correction for dynamic plate shrinkage in 2 ML of DMSO increases its ε_{mol} relative to 1 ML of DMSO. Whether area corrected or not, unique responses are obtained for the monolayer and multilayer, confirming experiments in bulk solvent.

Conclusion

The calculated capacitances and dielectric constants discussed above can only be viewed qualitatively because of the inherent assumptions and corrective factors. The simplest interpretation comes directly from the measured solvation data, which clearly indicate a larger, fundamentally different molecular response for 2 ML of DMSO compared to 1 ML of DMSO. A direct observation has been made in vacuum to confirm

a phenomenon postulated from bulk electrochemical measurements, and a connection between the fields of UHV and electrochemical surface science was reinforced.

Acknowledgements

This work was supported by the Director, Office of Science, Office of Basic Energy Sciences, Chemical Sciences Division of the U. S. Department of Energy, under Contract No. DE-AC02-05CH11231. The authors acknowledge NSF support for specialized equipment used in the experiments herein.

Supporting Information Available

A detailed description of the procedure used to fit the overlapping localized state and delocalized IPS at collection angles of 12° and 16° in a 2 ML coverage of DMSO is presented. Additionally, the slightly negative dispersion of the localized state is discussed. This information is available free of charge via the Internet at http://pubs.acs.org.

References

1. Bard, A. J.; Faulkner, L. R. *Electrochemical Methods*; John Wiley & Sons, Inc.: New York, NY, 1980; pp 488-549.

2. Kojima, H.; Bard, A. J. *J. Am. Chem. Soc.* **1975**, *97*, 6317.

3. Fawcett, W. R.; Levine, S. *J. Electroanal. Chem.* **1973**, *43*, 175.

4. Grahame, D. C. *Chem. Rev.* **1947**, *41*, 441.

5. Helmholtz, H. *Ann. Phys. Chem.* **1853**, *165*, 211.

6. Gouy, G. *J. Phys. Radium* **1910**, *9*, 457.

7. Chapman, D. L. *Phil. Mag.* **1913**, *25*, 475.

8. Stern, O. *Z. Elektrochem.* **1924**, *30*, 508.

9. Tanaka, M.; Gohda, Y.; Furuya, S.; Watanabe, S. *Jpn. J. App. Phys.* **2003**, *42*, L766.

10. Schröter, C.; Roelfs B.; Solomun, T. *Surf. Sci.* **1997**, *380*, L441.

11. Si, S. K.; Gewirth, A. A. *J. Phys. Chem. B* **2000**, *104*, 10775.

12. Borkowska, Z.: Stimming, U. In *Structure of Electrified Interfaces*; Lipkowski, J., Ross, P. N., Ed.; VCH: New York, NY, 1993; pp 277-307.

13. Sass, J. K.; Lackey, D.; Schott, J.; Straehler, B. *Surf. Sci.* **1991**, *247*, 239.

14. Borkowska, Z.: Stimming, U. In *Structure of Electrified Interfaces*; Lipkowski, J., Ross, P. N., Ed.; VCH: New York, NY, 1993; pp 309-400.

15. Weaver, M. J. *Int. J. Mass Spectrom.* **1999**, *182*, 403.

16. Verdaquer, A.; Sacha, G. M.; Bluhm, H.; Salmeron, M. *Chem. Rev.* **2006**, *106*, 1478.

17. Stähler, J.; Mehlhorn, M.; Bovensiepen, U.; Meyer, M.; Kusmierek, D. O.; Morgenstern, K.; Wolf, M. *Phys. Rev. Lett.* **2007**, *98*, 206105.

18. Güdde, J.; Berthold, W.; Höfer, U. *Chem. Rev.* **2006**, *106*, 4261.

19. Szymanski, P.; Garrett-Roe, S.; Harris, C. B. *Prog. Surf. Sci.* **2005**, *78*, 1.

20. Hotzel, A. *Prog. Surf. Sci.* **2007**, *82*, 336.

21. Zhao, J.; Li, B.; Onda, K.; Feng, M.; Petek, H. *Chem. Rev.* **2006**, *106*, 4402.

22. Liu, S. H.; Miller, A. D.; Gaffney, K. J.; Szymanski, P.; Garrett-Roe, S.; Bezel, I.; Harris, C. B. *J. Phys. Chem. B* **2002**, *106*, 12908.

23. Miller, A. D.; Bezel, I.; Gaffney, K. J.; Garrett-Roe, S.; Liu, S. H.; Szymanski, P.; Harris, C. B. *Science* **2002**, *297*, 1163.

24. Wandelt, K. In *Thin Metal Films and Gas Chemisorption*; Wissmann, P., Ed.; Elsevier: Amsterdam, New York, 1987; p 280.

25. Padowitz, D. F.; Merry, W. R.; Jordan, R. E.; Harris, C. B. *Phys. Rev. Lett.* **1992**, *69*, 3583.

26. Lingle, R. L.; Ge, N.-H.; Jordan, R. E.; McNeill, J. D.; Harris, C. B. *Chem. Phys.* **1996**, *205*, 191.

27. Gahl, C.; Bovensiepen, U.; Frischkorn, C.; Wolf, M. *Phys. Rev. Lett.* **2002**, *89*, 107402.

28. Bezel, I.; Gaffney, K. J.; Garrett-Roe, S. G.; Liu, S. H.; Miller, A. D.; Szymanski, P.; Harris, C. B. *J. Chem. Phys.* **2004**, *120*, 845.

29. Shipman, S. T.; Garrett-Roe, S.; Szymanski, P.; Yang, A.; Strader, M. L.; Harris, C. B. *J. Phys. Chem. B* **2006**, *110*, 10002.

30. Shirley, D. A. *Phys. Rev. B: Condens. Matter* **1972**, *5*, 4709.

31. Miller, T.; Hansen, E. D.; McMahon, W. E.; Chiang, T.-C. *Surf. Sci.* **1997**, *376*, 32.

32. Ikemiya, N.; Gewirth, A. A. *J. Phys. Chem. B* **2000**, *104*, 873.

33. Miller, A. D.; Gaffney, K. J.; Liu, S. H.; Szymanski, P.; Garrett-Roe, S.; Wong, C. M.; Harris, C. B. *J. Phys. Chem. A* **2002**, *106*, 7636.

34. Steinfeld, J. I.; Francisco, J. S.; Hase, W. L. *Chemical Kinetics and Dynamics*; Prentice-Hall, Inc.: Englewood Cliffs, NJ, 1989; pp 27.

35. Horng, M. L.; Gardecki, J. A.; Papazyan, A.; Maroncelli, M. *J. Phys. Chem.* **1995**, *99*, 17311.

36. Garrett-Roe, S.; Shipman, S. T.; Szymanski, P.; Strader, M. L.; Yang, A.; Harris, C. B. *J. Phys. Chem. B* **2005**, *109*, 20370.

37. Lindstrom, C.; Dutton, G.; Quinn, D. P.; Zhu, X.-Y. *Isr. J. Chem.* **2005**, *45*, 195.

38. Stähler, J.; Gahl, C.; Bovensiepen, U.; Wolf, M. *J. Phys. Chem. B* **2006**, *110*, 9637.

39. Zhu, X.-Y. *Annu. Rev. Phys. Chem.* **2002**, *53*, 221.

Table 1: Linear slopes of n=1 IPS energy relaxation for 1 ML of DMSO at various collection angles

	0°	4°	8°	12°	16°	20°	24°
Slope (eV/ps)	-.25	-.26	-.25	-.26	-.30	-.33	-.32

Table 2: Average of rise and decay times of n=1 IPS for 2 ML of DMSO

	12°	16°	20°	24°
τ (fs)	105	106	85	68

Table 3: Electrochemical Model Predictions for 1 ML and 2 ML of DMSO

	1 ML	2 ML
Cap at t=0 (F)	6.0×10^{-20}	5.6×10^{-20}
Cap/A at t=0 (F/ cm^2)	7.7×10^{-8}	7.2×10^{-8}
Cap at $t \rightarrow \infty$ (F)	$6.1\text{-}6.3 \times 10^{-20}$	6.1×10^{-20}
Cap/A at $t \rightarrow \infty$ (F/cm^2)	$7.8\text{-}8.0 \times 10^{-8}$	9.3×10^{-7}
ε_{mol}	.034-.091	.18
ε_{mol}(A corr)	.034-.091	26

Cap = capacitance; Cap/A = capacitances per unit area; ε_{mol} = dielectric constant; ε_{mol}(A corr) = area corrected dielectric constants

Figure 1: The dynamics of the n=1 IPS are displayed for 1 ML (left column) and 2 ML (right column) coverages of DMSO on Ag(111) at signal collection angles of 0° and 24°. Photoelectron signal intensity is indicated by color from most intense (red) to zero (blue).

Figure 2: A 2PPE dosing survey of DMSO on Ag(111) is presented. The data was collected at the 1 ML voltage bias, and the spectra have not been corrected for inelastic scattering. Intensity has been scaled, and a vertical offset has been added to present the data on one graph.

Figure 3: 2PPE spectra of 1 ML of DMSO are displayed at zero and long pump-probe delay times at a range of collection angles. Intensity has been scaled, and a vertical offset has been added to present the data on one graph.

Figure 4: The photoelectron count intensity is plotted for the delocalized 1 ML DMSO n=1 IPS at 0° and 24° and the localized 2 ML n=1 IPS at 24°. Dots represent the actual data, and solid lines represent the fits. Intensity has been scaled to present the data on one graph.

Figure 5: The n=1 IPS dynamic energy relaxation is displayed for 1 ML and 2 ML of DMSO collected at 0°. Delocalized and localized features cannot be resolved for the 2 ML coverage at 0°, and the sum of both contributions was fit to one peak. The 2 ML binding energy, therefore, primarily reflects the delocalized solvation response at early times and the localized solvation response at long times, which is dictated by the relative populations.

Figure 6: 2PPE spectra of 2 ML of DMSO are displayed at zero, intermediate and long pump-probe delay times at a range of collection angles. Intensity has been scaled, and a vertical offset has been added to present the data on one graph. A vertical line has been added at the 0° n=1 binding energy as a guide for the eye.

Figure 1: Time-resolved 2PPE of 1 ML and 2 ML DMSO coverages

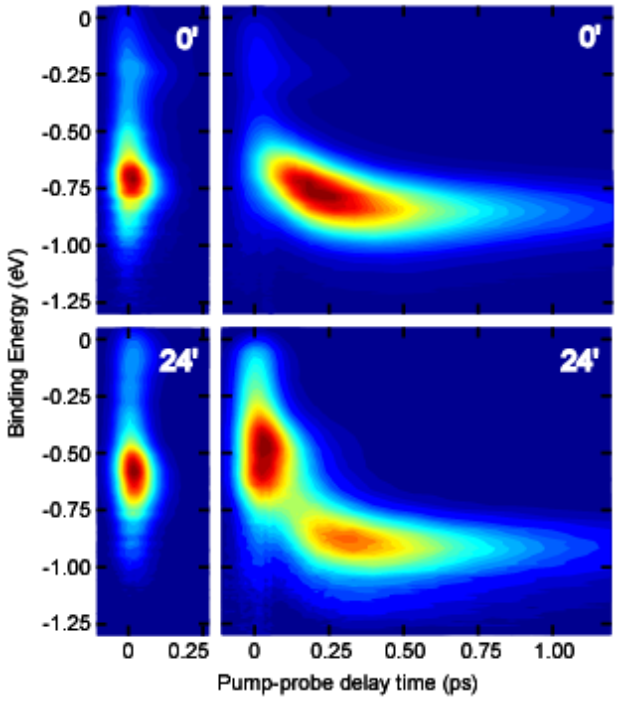

Figure 2: Dosing survey of DMSO with 2PPE

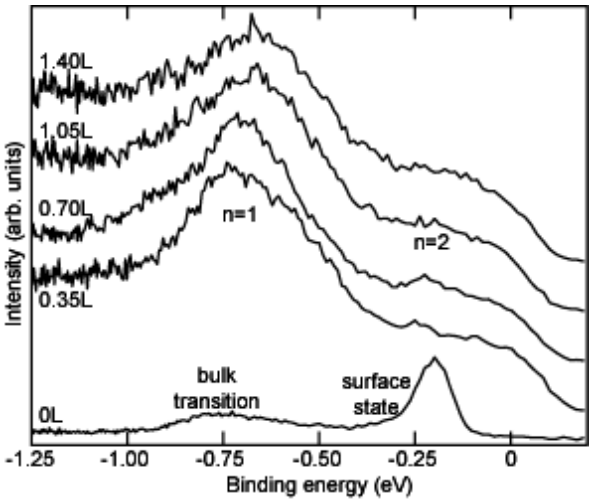

Figure 3: Dispersion of 1 ML DMSO

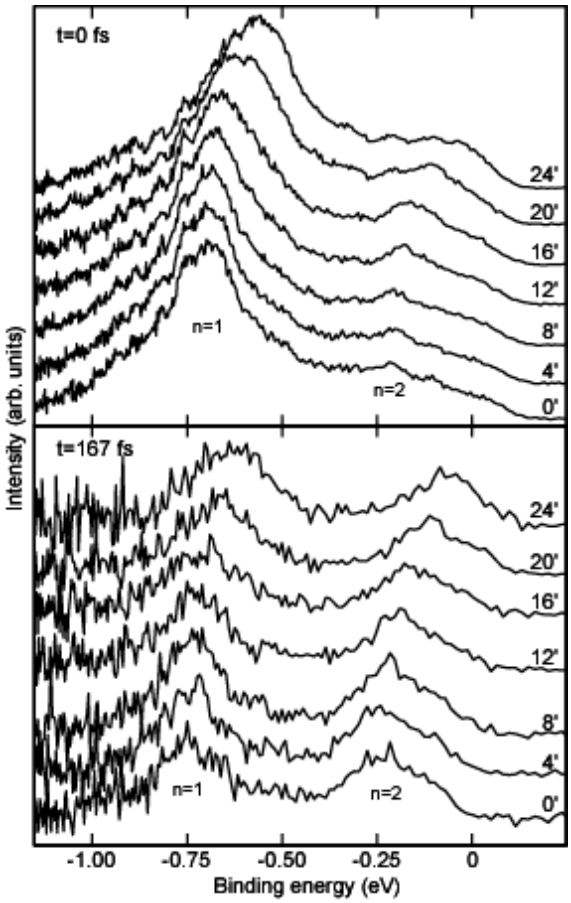

Figure 4: Population dynamics of the n=1 IPS in 1 ML and 2 ML DMSO

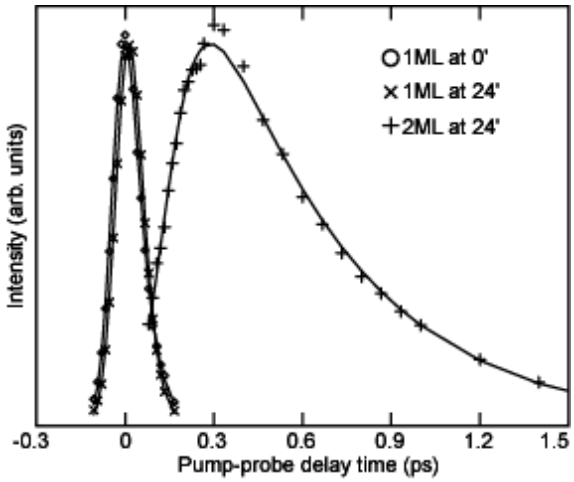

Figure 5: Solvation response of 1 ML and 2 ML DMSO to the n=1 IPS

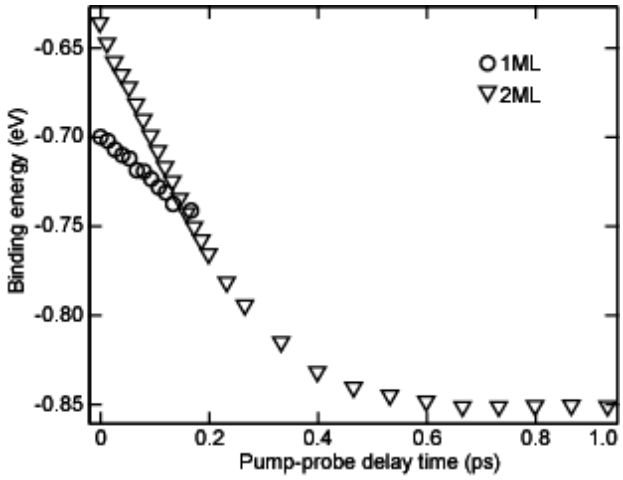

Figure 6: Dispersion of 2 ML DMSO at various pump-probe delay times